

# Co-published by Institute of Fluid-Flow Machinery Polish Academy of Sciences

# **Committee on Thermodynamics and Combustion**

Polish Academy of Sciences

Copyright©2025 by the Authors under licence CC BY-NC-ND 4.0

http://www.imp.gda.pl/archives-of-thermodynamics/



# Simplified dynamic heat exchanger models for heat recovery steam generators

Nabil Youssef<sup>a,b\*</sup>, Assaad Zoughaib<sup>a</sup>, Valentin Drouet<sup>b</sup>

aMines Paris – PSL, 60 Boulevard Saint Michel, 75006 Paris, France bMetroscope, 63 Boulevard Haussmann, 75008 Pairs, France \*Corresponding author email: nabil.youssef@metroscope.tech

Received: 30.12.2024; revised: 05.02.2025; accepted: 09.02.2025

# **Abstract**

Monitoring power plants necessitates sophisticated methods and reliable dynamic models, especially with the increasing flexibility demand. The primary challenge of this work is to develop a modelling strategy for heat recovery steam generators (HRSG) that enables simple yet accurate simulation of their dynamic behaviour, accounting for the delayed response of their heat exchangers to load variations caused by high thermal inertia. The proposed modelling methodology aims to build models suitable for monitoring power plants based on a set of sensor measurements, which can realistically be found in a power plant. This approach eliminates the need for extensive system design information, which may not always be accessible to the modeller. First, fully detailed, pseudo three dimensional Modelica model of the monophasic heat exchangers is developed. The model is then simplified progressively while the impact on accuracy is assessed. A more simplified model is later developed by assuming a lumped global heat transfer coefficient and a mass. The simplified model provides promising results, demonstrating a good compromise between simple calibration process and accuracy. A model of the evaporator is also presented and validated based on literature. Finally, a qualitative analysis of the full HRSG model is conducted. The dynamic behaviour as well as the time constants of the heat exchangers are analysed. The results demonstrate a good agreement with the expected physical behaviour.

**Keywords:** Dynamic modelling; Steam generation; Heat exchanger; Model calibration; Model reduction

Vol. 46(2025), No. 2, 185-197; doi: 10.24425/ather.2025.154197

Cite this manuscript as: Youssef, N., Zoughaib, A., & Drouet, V. (2025). Simplified dynamic heat exchanger models for heat recovery steam generators. *Archives of Thermodynamics*, 46(2), 185–197.

# 1. Introduction

Power generation is simultaneously the largest carbon dioxide emitter and a key driver in the transition to zero emissions. This is insured by a rapid expansion of renewable energy sources, which are expected to overtake coal as the largest source in 2025 [1]. The net additions to renewable energy capacity are dominated by wind and solar, which are inherently variable, contributing to a fluctuating feed-in power to the grid. This poses a challenge to grid operators in maintaining the load and supply balance [2].

Several solutions, such as energy storage and operational flexibility, are being deployed. Existing conventional power plants, like combined cycle gas turbines (CCGTs), will operate alongside renewable energies to ensure flexibility from the supply side in the short to medium term.

CCGT power plants offer a combination of advantages compared to other types of power plants, such as high efficiency, including during part load operations, fast start-up and good operational flexibility [3]. However, the dynamic flexibility of CCGT is restricted by its heat recovery steam generator (HRSG) because of its thick-walled components, requiring more transi-

#### **Nomenclature**

A – heat exchange area, m<sup>2</sup>

 $C_p$  – specific heat capacity at constant pressure, J/(kg K)

D - diameter, m

e – thickness, m

g – gravitational acceleration, m/s<sup>2</sup>

H – height, m

h – specific enthalpy, J/(kg K)

k – heat transfer coefficient, W/(m² K)

l – water level, m

L – length, m

 $\dot{m}$  – mass flow rate, kg/s

m - mass, kg

*n* – number of discretization elements

 $N_r$  – number of rows

Nu - Nusselt number

P – pressure, Pa

Pr - Prandtl number

 $\dot{q}$  - heat flow, W

r – radius, m

 $r_{UA}$  – ratio

Re - Reynolds number

S – pitch, m

t - time, s

T - temperature, K

 $\bar{T}$  – average temperature, K

u – specific internal energy, J/(kg K)

√ – flow speed, m/s

U - overall heat transfer coefficient, W/(m<sup>2</sup> K)

V − volume, m<sup>3</sup>

 $x_r$  – steam quality at the riser outlet

 $\overline{x_v}$  – average volume fraction in the riser

#### **Greek letters**

 $\alpha$  – thermal diffusivity, m<sup>2</sup>/s

 $\beta$  – constant parameters in drum equations

ζ – friction coefficient

η – efficiency

 $\lambda$  – thermal conductivity, W/(m K)

 $\mu$  – dynamic viscosity, kg/(m s)

 $\rho$  – density, kg/m<sup>3</sup>

 $\tau$  – time constant, s

#### **Subscripts and Superscripts**

a - air

c – condensation

conv-convection

d – drum

e – along tube thickness

f – fins

fg – flue gas

fw - feedwater

i – inner side of the tube

in - inlet

l – longitudinal

o – outer side of the tube

out - outlet

*n* − time step number

r - riser

s – steam

t – transversal

tot - total

w – water

wall- tubes wall

z – along tube length

# **Abbreviations and Acronyms**

HRSG - heat recovery steam generator

CCGT - combined cycle gas turbine

HP – high pressure

IP – intermediate pressure

LP - low pressure

Eco – economizer

tion time.

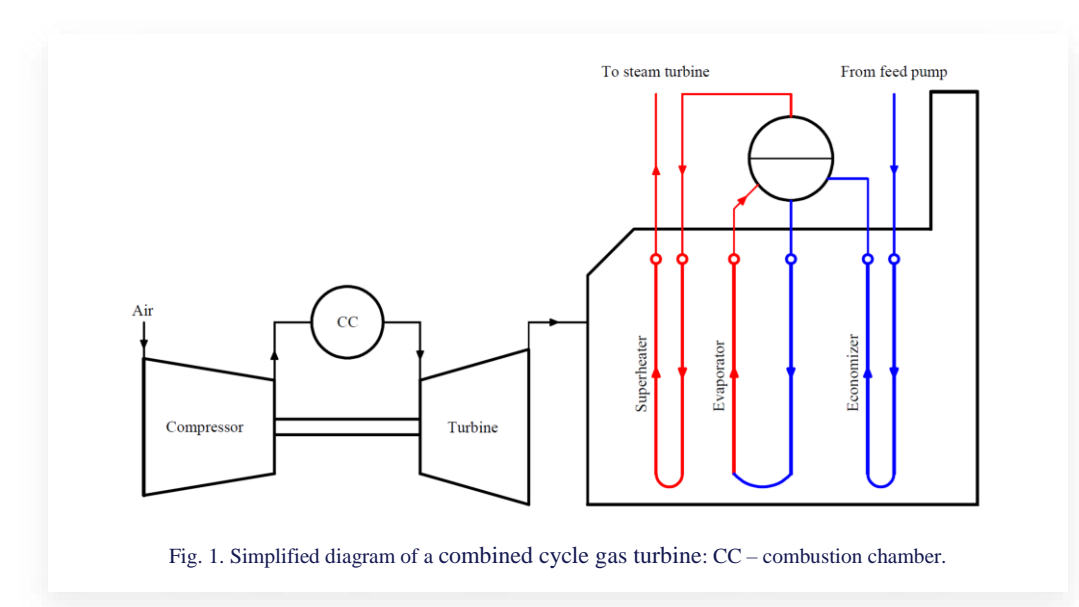
The increasing frequency of flexible operation modes in power generation assets promotes the use of digital solutions to help maintain safety, availability, and efficiency. In [4,5], dynamic models are developed to improve the start-up time of a CCGT while assessing the state of stressed components to maintain safe operation. In [6], two models are compared to estimate the reduction of the residual life of a CCGT power plant due to its flexible operation. It states that load cycling triggers damage, failures, and frequent unplanned maintenance work. In [7], dynamic simulations are carried out to highlight the advantages of a new hybrid once-through and natural circulation HRSG over conventional natural circulation ones. Moreover, model-based and model-free fault detection and diagnosis techniques are applied to prevent power generation losses and extended downtimes, such as in [8,9]. Models presented in the literature often rely heavily on detailed design information. While this dependence can improve their accuracy, it also introduces challenges such as increased calibration complexity and slower simulation times. These factors can limit their scalability and

applicability in scenarios where comprehensive design data is not available or where computational efficiency is critical.

In this study, a modelling methodology of the HRSG is presented. Figure 1 shows a diagram of a simplified CCGT. The HRSG is placed at the gas turbine's exhaust to recover the remaining energy contained in the hot flue gases. It is composed of a series of heat exchangers. Water flows inside the tubes while the hot flue gas flows from the outside. Three main types of heat exchangers are used:

- Economizer: liquid water is heated to a point near saturation;
- Evaporator: liquid water is evaporated in once-through or drum-type evaporators [10];
- Superheaters: steam is superheated before it is sent to steam turbines to maximize efficiency while respecting the mechanical limits of the blades.

In economizers and superheaters, water flows as a singlephase fluid, liquid, or steam, while in evaporators, phase change occurs. Single-phase heat exchangers dominate the space of the



HRSG, and temperature gradients happen in both fluids across the tubes. Depending on the phase of the water and the exchange surface, the global heat transfer coefficient can be limited from the flue gas or the liquid water sides. However, in two-phase heat exchangers, the heat transfer coefficient on the water side is much higher than that of the flue gas, making the latter the limiting side. The temperature of the mixture is constant during the phase change, so the temperature gradient is present only on the flue gas side. Nevertheless, hydrodynamics plays a critical and complex role in evaporators, particularly in natural circulation evaporators, and this aspect will be discussed in detail later in the paper.

In HRSG, each heat exchanger is composed of a number of rows  $(N_r)$  of finned tubes to enhance heat exchange: Headers at both ends of the tubes bundle are used to distribute the water/steam or mix it, as shown in Fig. 2. In one-pass heat exchangers, water flows in the same direction in each row of tubes as seen in Fig. 3a. However, in multiple pass heat exchangers, water changes its direction throughout the row, by separators placed in the upper and lower headers, as in Fig. 3b.

While the HRSG is globally a counter-flow system, each individual tube row functions as a crossflow heat exchanger. Modelling the dynamic response of heat exchangers in the HRSG, especially when the gas turbine load varies, requires detailed information about their design and properties.

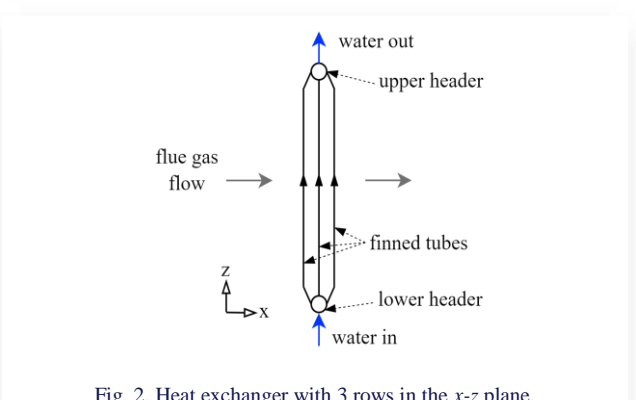
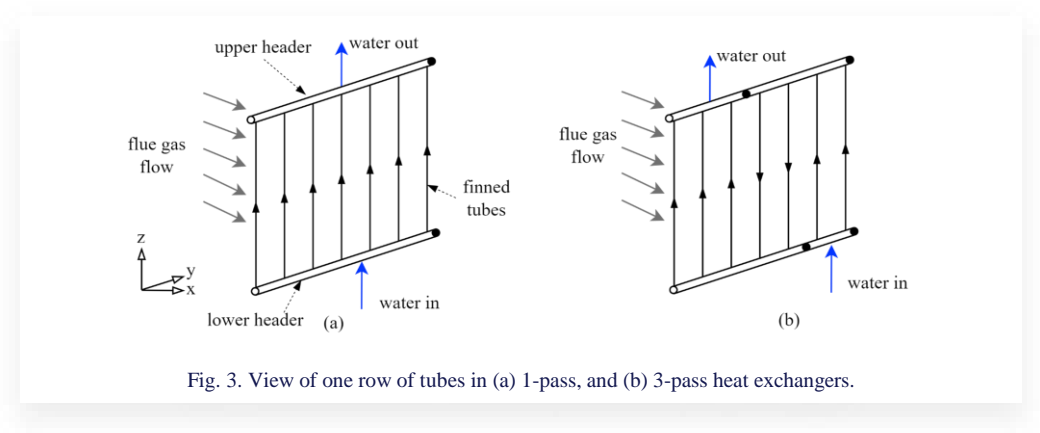


Fig. 2. Heat exchanger with 3 rows in the x-z plane.

The objective of this work is to develop a simplified model of the HRSG, balancing the complexity and accuracy. The methodology and results are divided into three sections. In the first one, starting from a fully detailed, pseudo three-dimensional model, a simplified monophasic heat exchanger model is developed. The simplification steps and their impact on the accuracy of the model, both on steady-state, and dynamic responses are analyzed. In the second section, a model of a natural recirculation evaporator-drum system is presented in detail. It is based on a well-known publication in literature. Validation was performed through comparison with results reported in the literature. Finally, in the third section, a full model of an industrial



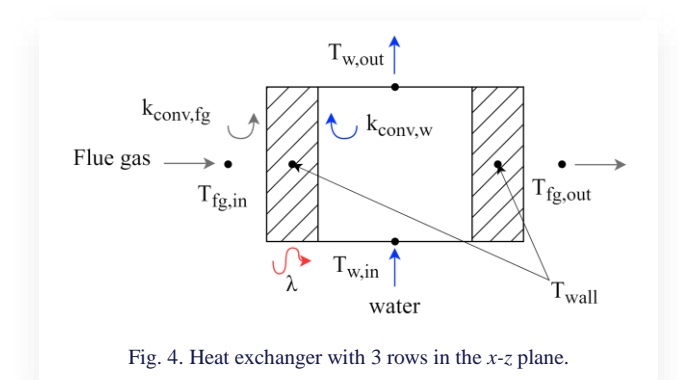
HRSG is developed. The dynamic response is studied by introducing perturbation to the boundary conditions. The time constants of different heat exchangers are outlined.

# 2. Monophasic heat exchanger modelling

In this section, a mathematical model of a single-phase dynamic heat exchanger is presented with the possible discretization strategies and main assumptions. Then, a sensitivity analysis is conducted on various discretization parameters, as well as an assessment of simplification assumptions impact on the model's precision on both the steady-state and dynamic behaviours. Finally, a simplified model based on an overall heat transfer coefficient and a lumped mass is developed. This model necessitates the specification of a predefined ratio of heat transfer coefficients that can be estimated without precise knowledge of the design of the heat exchangers. The impact of this ratio on the model's outputs is studied to define the validity range. The main mathematical equations, modelling assumptions, and empirical correlations employed in the model are outlined. Finally, the discretization strategy of the heat exchanger model across different directions is described.

#### 2.1. Heat exchange model

In this section, the main mathematical equations used to describe the monophasic heat exchange are listed. One tube element is considered with average properties on the flue gas and the water side, as shown in Fig. 4.



First, dynamic mass balance is applied on water and flue gas, respectively:

$$V_{w}\frac{d\rho_{w}}{dt} = \dot{m}_{w,in} - \dot{m}_{w,out},\tag{1}$$

$$V_{fg}\frac{d\rho_{fg}}{dt} = \dot{m}_{fg,in} - \dot{m}_{fg,out}, \tag{2}$$

where V represents the constant volume of the tubes and channels,  $\dot{m}$  — the mass flow rate,  $\rho$  — the density, and t — the time. Subscripts w and fg denote water and flue gas, respectively, while the subscripts in and out indicate inflow and outflow. The time variation of density can be neglected due to its minimal impact on the mass flow rate. Therefore, in Eqs. (1) and (2), terms  $\frac{d\rho_w}{dt}$  and  $\frac{d\rho_{fg}}{dt}$  can be neglected.

The energy balances on both sides are given by

$$V_{w} \frac{d(\rho_{w} u_{w})}{dt} = \dot{m}_{w,in} h_{w,in} - \dot{m}_{w,out} h_{w,out} + \dot{q}_{w}, \qquad (3)$$

$$V_{fg} \frac{d(\rho_{fg}u_{fg})}{dt} = \dot{m}_{fg,in} h_{fg,in} - \dot{m}_{fg,out} h_{fg,out} + \dot{q}_{fg}, \quad (4)$$

where u represents the specific internal energy, h – the specific enthalpy, and q – the heat flow.

The energy balance on the tube's wall is given by

$$\dot{q}_w + \dot{q}_{fg} + m_{wall} C_{p,wall} \frac{dT_{wall}}{dt} = 0, \tag{5}$$

where m represents the mass,  $C_p$  – the specific heat, and T – the temperature. Subscript wall denotes the tubes wall.

The heat capacities of water and flue gas are negligible in comparison to the capacity of the metal. Consequently, the terms  $\frac{d(\rho_W u_W)}{dt}$  and  $\frac{d(\rho_{fg} u_{fg})}{dt}$  in Eq. (3) and (4) can be neglected. Given that the pressure drop in a monophasic flow exerts a minor influence on the heat transfer, this phenomenon will be ignored in this model.

Convection heat transfer equations are applied on water and flue gas sides. The heat flow of water  $\dot{q}_w$  and flue gas sides  $\dot{q}_{fg}$  are computed by

$$\dot{q}_{w} = k_{conv.w} A_{i} (T_{wall} - \bar{T}_{w}), \tag{6}$$

$$\dot{q}_{fg} = k_{conv,fg} \left( T_{wall} - \bar{T}_{fg} \right) \left( A_o + \eta_f A_f \right). \tag{7}$$

In these equations,  $k_{conv}$  represents the convection heat transfer coefficient, A the surface and  $\eta$  the efficiency. Subscripts i and o refer to the inner and outer smooth sides of the tube, respectively, while f denotes fins. Since heat is transferred from flue gas to water, it is expected that  $\dot{q}_w > 0$  and  $\dot{q}_{fg} < 0$ . The mean temperatures  $\overline{T}_w$  and  $\overline{T}_{fg}$  are computed by

$$\bar{T}_w = \frac{T_{w,in} + T_{w,out}}{2},\tag{8}$$

$$\bar{T}_{fg} = \frac{T_{fg,in} + T_{fg,out}}{2}.$$
 (9)

The convection heat transfer coefficients are computed according to empirical correlations. First, the Reynolds (Re) and Prandtl (Pr) numbers are calculated for both water and flue gas sides as

$$Re = \frac{\rho v D}{\mu},\tag{10}$$

$$Pr = \frac{c_p \mu}{\lambda},\tag{11}$$

where  $\nu$  represents the velocity, D – the diameter,  $\mu$  – the dynamic viscosity and  $\lambda$  – the thermal conductivity.

For water, the Dittus-Boelter [11] correlation is applied as

$$Nu_w = 0.023 Re_w^{0.8} Pr_w^{0.4},$$
 (12)

where Nu is the Nusselt number.

For the flue gas side, the Escoa (Extended Surface Corporation of America) correlation [12] is used to calculate the external convection heat transfer coefficient for segmented finned-tubes at staggered arrangement:

$$Nu_{fg} = C_1 C_3 C_5 Re_{fg} Pr_{fg}^{0.33} \left(\frac{T_{fg}}{T_f}\right)^{0.25} \left(\frac{D_f}{D_o}\right)^{0.5}, \quad (13)$$

where  $C_1 = 0.25 \text{Re}^{-0.35}$ ,  $C_3 = 0.55 + 0.45 \exp\left(\frac{0.35 H_f}{S_f - e_f}\right)$  and  $C_5 = 0.7 + [0.7 - 0.8 \exp(-0.15 N_r^2)] \exp\left(-\frac{S_l}{S_t}\right)$ , H is the height, S – the pitch, e – the thickness,  $N_r$  – the number of rows. Subscripts l and t denote longitudinal and transverse, respectively.

Knowing the Nusselt number for each fluid, the convection heat transfer coefficients can finally be calculated by

$$k_{conv} = \text{Nu} \frac{\lambda}{\rho}.$$
 (14)

Heat is transferred from the flue gas to the water through the tube's wall by conduction. Assuming that heat transfer is only in one direction, the following can be applied:

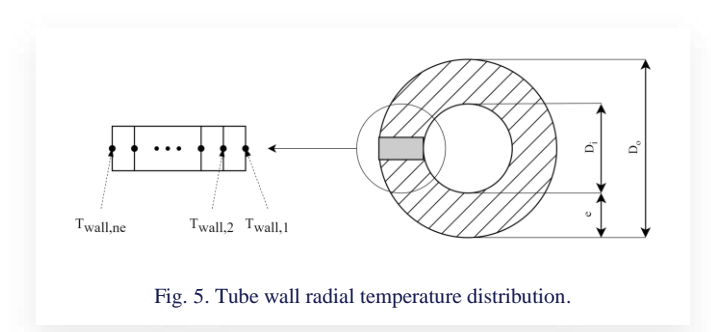
$$\frac{1}{\alpha} \frac{\partial T}{\partial t} = \frac{1}{r} \frac{\partial}{\partial r} \left( r \frac{\partial T}{\partial r} \right), \tag{15}$$

where  $\alpha$  is the thermal diffusivity and r is the radius.

The time constant  $\tau$  is an important parameter to characterize a transient phenomenon. It represents the time a system takes to achieve approximately two-thirds of its final equilibrium value in response to a perturbation of an input [13]. This parameter will be used to evaluate the dynamic response of the models later in the paper.

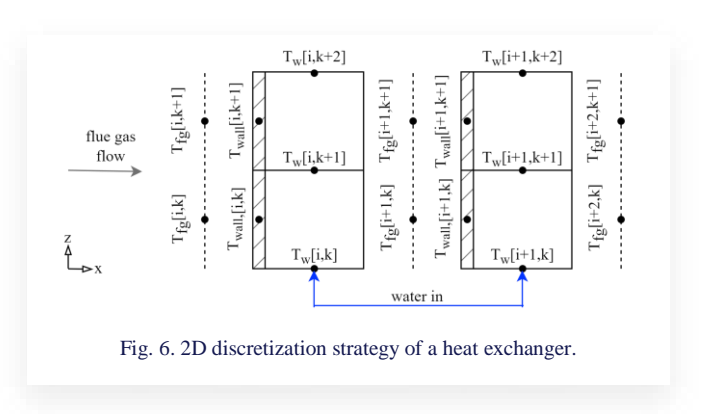
#### 2.2. Discretization

The wall is discretized into  $n_e$  elements to capture the temperature distribution along the tubes' thickness as seen in Fig. 5. In Eqs. (6) and (7),  $T_{wall}$  is substituted with that of the corresponding node temperature on the side of the fluid. For instance,



in Eq. (6), heat is exchanged through the inner surface of the tube, so  $T_{wall,1}$  is used.  $T_{wall,ne}$  is used in Eq. (7). Equation (15) is then solved for the tube nodes.

The fluid properties in the heat exchanger vary in a non-linear way. Therefore, it is necessary to discretize it in small control volumes to ensure high accuracy [14]. In this case, several tube elements are assembled. Figure 6 shows the 2D discretization of a section of a heat exchanger. Flue gas flows across the tube bundle from left to right, while water flows upwards inside the tubes. Tubes are divided into  $n_z$  elements along the tube length. Two main assumptions are considered: (1) the flue gas does not mix between the different elements in the tube length direction, (2) all tubes, in parallel, in the same row (y-direction



in Fig. 3) with the same water flow direction have identical temperature evolution along the tube length.

The dynamic heat exchanger model is developed using Modelica [15], an object-oriented, equation-based language, powerful to model complex systems containing multi-physics components with a causal connection between them. Dymola [16], a multi-engineering modelling and simulation software based on Modelica, is used to build and simulate this model. This model is developed within Metroscope Modeling Library (MML) [17], which contains the necessary components for the thermodynamic modelling of CCGTs and the secondary cycles of nuclear power plants.

# 2.3. Sensitivity analysis on discretization strategy and simplification assumptions

The impact of varying the discretization parameters of the heat exchanger is detailed. Moreover, some simplification assumptions are investigated to ensure that the model keeps an acceptable precision. Both the steady state and dynamic responses are investigated on one heat exchanger, then on two consecutive heat exchangers. The models are initialized under steady state conditions. At t = 100 s, a sudden decrease of  $20^{\circ}$ C in the flue gas temperature is applied to trigger a dynamic response, mimicking a load decrease of the turbine. Then, a sensitivity analysis is performed for each assumption. Validation is performed on the outlet water temperature of the exchanger, as it is typically the only measured property on an industrial HRSG: the convergence value is used to validate the steady-state response, and the time constant is used to validate the dynamic response.

#### 2.3.1. Impact on one heat exchanger

A typical high pressure superheater is considered with the following boundary conditions at its inlet: flue gas side  $T = 630^{\circ}\text{C}$ , P = 1 bar,  $\dot{m} = 660$  kg/s and on the water side  $T = 250^{\circ}\text{C}$ , P = 120 bar and  $\dot{m} = 84$  kg/s. The main design specifications of this superheater are: tubes length L = 22 m, tubes outer diameter  $D_o = 40$  mm, tubes wall thickness e = 3 mm, heat exchanger mass m = 38 200 kg, number of rows  $N_r = 2$ , number of tubes per row of 180, transversal pitch of 75 mm, longitudinal pitch of 95 mm, fins efficiency of 0.8 and fins pitch of 9.5 mm.

**Tube wall temperature distribution.** As discussed in Section 2.2, the wall is discretized into several elements. The reference model for this sensitivity analysis has 5 temperature nodes.

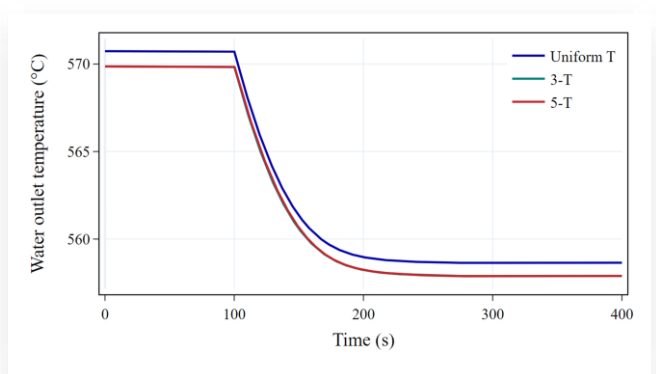


Fig. 7. Evolution of water outlet temperature for the 3 cases of tube wall temperature distribution.

Two other cases are investigated: one with a uniform temperature and the other with 3 temperature nodes. Figure 7 shows the simulation results of the 3 cases. The uniform temperature model presents a steady state error of 0.87°C compared to the 5 nodes model. However, the 3 nodes model shows no error in the steady state response compared to the 5 nodes model, as their curves overlap. This low error was expected due to the thin tube walls and the low Biot number.

The reference model of 5 nodes has a time constant of 36.7 s, while the models with uniform temperature and 3 nodes have 35.9 s and 36.0 s, respectively. Therefore, 0.8 s and 0.7 s errors are induced by each of the two models. According to the data acquisition frequency (typically 1 s), these errors can be considered insignificant. This dynamic error is due to the variations in the repartition of the energy stored in the wall. Thus, a model with 3 nodes appears to be enough to provide accurate steady state and dynamic responses.

**Discretization along the tube length.** A sensitivity analysis is performed on the number of elements  $n_z$  used to discretize the tubes. Figure 8 shows the steady-state and the dynamic impacts of varying  $n_z$  from 1 to 15 on the model's outputs. Considering the case with  $n_z = 15$  as a reference, the outlet temperature error decreases rapidly from 3.61°C to 0.19°C as the number of elements increases from  $n_z = 1$  to  $n_z = 4$ , before stabilizing close to zero. Similarly, the time constant error follows the same trend, decreasing from 7.62 s at  $n_z = 1$  to 0.4 s at  $n_z = 4$ . This error is induced by the non-linear evolution of the steam's temperature throughout the finned tube. Therefore, for

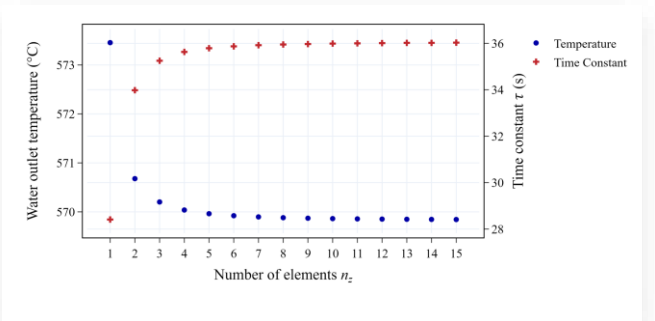
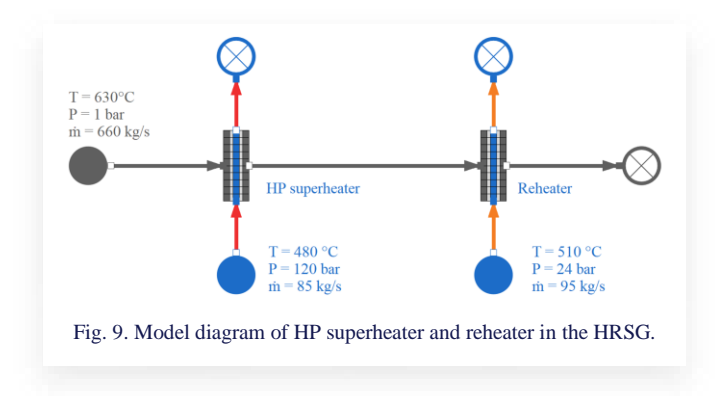


Fig. 8. Sensitivity analysis of element count  $n_z$  on steady-state and dynamic responses.

this heat exchanger, a model with  $n_z = 4$  is considered satisfactory compared to the sensors measurements uncertainties.

# 2.3.2. Impact on two consecutive exchangers

In HRSG, the flue gas flows through multiple heat exchangers. Therefore, it is also essential to study the dynamic response of a series of exchangers. For this purpose, a reheater is connected to the outlet of the high pressure (HP) superheater, as shown in Fig. 9. This time, the water outlet temperature, and the time constant of the reheater are used as quantities of interest to assess the model's precision under various assumptions.



**Fuel gas temperature distribution.** When the heat exchanger is discretized along the tube length, the flue gas temperature distribution between both heat exchangers can be computed. In this section, the impact of mixing the flue gas flow before entering the second heat exchanger is assessed. Three different cases are compared, all having an element count along the tube length  $n_z = 4$ , as suggested in the previous section:

- Case 1: no flue gas mixing and water flows in the same direction in both heat exchangers (as seen in Fig. Fig. 9);
- Case 2: no flue gas mixing and water in the reheater flows in the opposite direction compared to the superheater (downwards);
- Case 3: flue gas is mixed between the heat exchangers, thus the water flow direction is irrelevant.

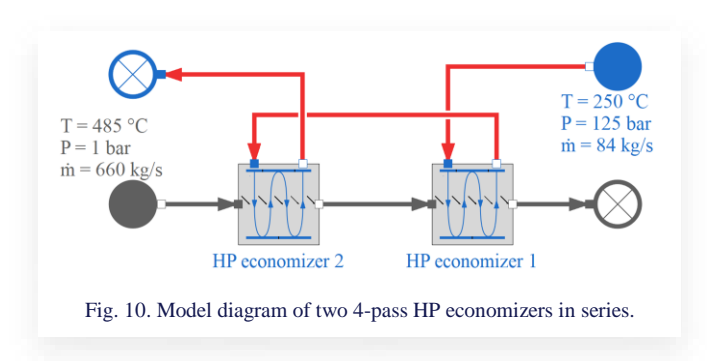
Table 1 displays the simulation results of the reheater for the 3 cases. Analysing the water outlet temperature of the reheater, case 3 presents 1.40 and 1.43°C gaps compared to cases 1 and 2, respectively. On the dynamic level, 0.33 and 0.24 s time constant errors are calculated compared to cases 1 and 2, respectively. This section shows that averaging the flue gas temperature between heat exchangers, while maintaining an appropriate elements count, can give interesting precision levels, regardless of the water flow direction. The acceptability of this precision depends on the uncertainty of the available measurements, as well

Table 1. Reheater simulation results of the 3 cases.

	$T_{w,out}$ (°C)	τ (s)
Case 1	580.36	38.86
Case 2	577.53	38.29
Case 3	578.96	38.53

as the application requirements. Moreover, in a real exchanger, depending on the turbulence of the flue gas, which is enhanced by the fins and the tubes spacings, some mixing occurs.

**Single pass assumption.** As shown in Fig. 3, water can undergo a single or multiple passes through the heat exchanger. Considering the number of passes complicates the model and requires accurate design information of the heat exchanger. In this section, the impact of assuming a multiple-pass heat exchanger as a single pass one on two consecutive heat exchangers is evaluated. Two 4-pass HP economizers in series are considered, as seen in Fig. 10.



The reference case has  $n_z=10$  and a 2D flue gas temperature distribution between the heat exchangers. Two simplification cases are studied:

- Case 1:  $n_z = 10$ , 4-pass heat exchanger models, and an averaged flue gas temperature between both economizers;
- Case 2:  $n_z = 10$ , equivalent single pass heat exchanger models, and an averaged flue gas temperature between both economizers.

Table 2 presents the results for the reference model, as well as the two cases. The errors in the water outlet temperatures for both cases are significantly less than 0.1°C. Similarly, only case 2 presents a time constant error of 0.1 s. This section suggests that simplifying multi-pass heat exchangers into single-pass ones is a plausible assumption.

We conclude from the previous study that the discretization along the tube length is necessary in modelling dynamic heat exchangers. Averaging flue gas temperature between heat exchangers in series is an acceptable assumption. Moreover, a three nodes discretization of the tube wall is enough to capture the temperature distribution in the wall and its impact of the time constant. Finally, multi-pass heat exchangers can also be replaced by equivalent single-pass ones with negligible impact on the model's output accuracy. In the next section, the impact of further simplifications is assessed to facilitate easier calibration.

Table 2. Simulation results of the 3 models of 2 multi-pass economizers in series.

Model	Eco1 <i>T<sub>w,out</sub></i> (°C)	Eco2 T <sub>w,out</sub> (°C)	Eco1 τ (s)	Eco2 τ (s)
Ref.	289.6	321.1	55.4	73.0
Case 1	289.6	321.1	55.4	73.0
Case 2	289.6	321.1	55.3	73.0

# 2.4. Simplified model

As previously stated, the detailed model requires design information that might not always be available to the modeller. Models of existing power plants require calibration based on site data. However, calibration of such models is also complex due to the considerable number of parameters that need to be adjusted for each heat exchanger. In addition, the simulation of complex models with fine discretization requires high computational resources. Therefore, a simplified model of a single monophasic heat exchanger is introduced based on the results of Section 2.3 to overcome these limitations. It is built to be easily calibrated, with a focus on the precision measurable quantities in actual HRSG.

# 2.4.1. Heat exchange model

Instead of computing the convection and conduction heat transfer coefficients, an overall heat transfer coefficient (U) is used. If the design information is available, it can be computed by

$$\frac{1}{UA} = \frac{1}{(UA)_W} + \frac{1}{(UA)_{fg}},\tag{16}$$

where *A* is the heat exchange surface.

The ratio  $(r_{UA})$  between the overall heat transfer coefficients of the water and flue gas sides is introduced. It is calculated as

$$r_{UA} = \frac{(UA)_W}{(UA)_{fg}}. (17)$$

The heat flows for the water and flue gas sides are calculated by, respectively:

$$\dot{q}_w = (UA)_w (T_{wall} - \bar{T}_w), \tag{18}$$

$$\dot{q}_{fg} = (UA)_{fg} \left( T_{wall} - \bar{T}_{fg} \right). \tag{19}$$

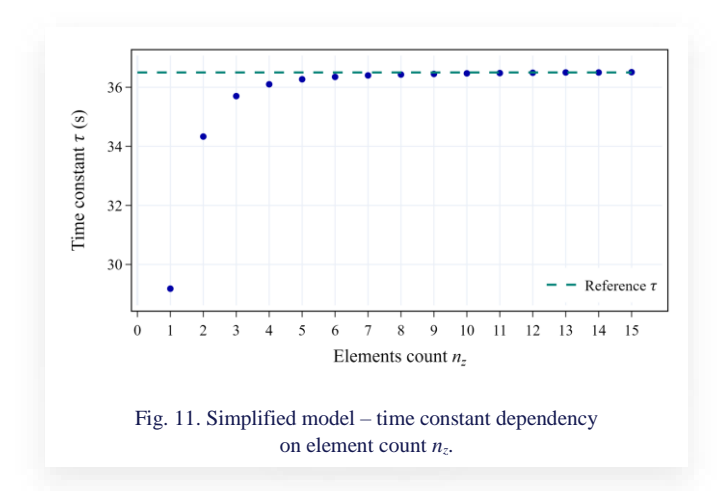
The tube wall temperature is considered uniform along the tube's thickness. The energy balance on the tube's wall is the same as in Eq. (5).

# 2.4.2. Calibration and discretization

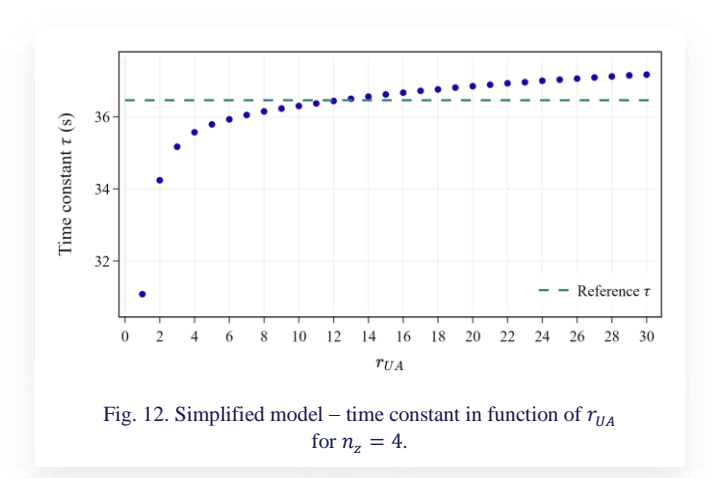
The steady-state calibration of the simplified model consists of imposing  $T_{w,out}$  and  $r_{UA}$  calculated by a reference model (superheater model with  $n_z=10$ ) and getting the UA as an output. The simplified model is discretized along tube length, therefore, for each element count  $n_z$ , a separate calibration simulation is conducted. At the end of the calibration process, the simplified models with different  $n_z$  values, give all the same steady-state response as the reference model since they were calibrated with the same  $T_{w,out}$ . However, the dynamic response represented by the time constant  $\tau$  depends on  $n_z$ , as seen in Fig. 11. The reference  $\tau$  is equal to 36.46 s, consequently, the error is reduced to less than 0.5 s when  $n_z$  is equal or greater than 4.

#### 2.4.3. Sensitivity analysis on $r_{IIA}$

Without the detailed design information of the heat exchanger, ratio  $r_{UA}$  cannot be determined. For this purpose, this section conducts a sensitivity analysis on the ratio  $r_{UA}$  to assess the im-



pact of an error in a guessed value on the outputs of the model. A model with  $n_z = 4$  is considered. The ratio  $r_{UA}$  is varied between 1 and 30. The reference model computes a ratio  $r_{UA} = 7.54$  for the HP superheater. Figure 12 shows that the time constant depends on  $r_{UA}$ . However, compared to the reference  $\tau$ , choosing a ratio  $r_{UA}$  higher than 4 keeps the time constant error less than 1 s. Therefore, an approximation of the ratio  $r_{UA}$  for each type of heat exchanger can give a satisfactory dynamic response simulation. Ideally, this ratio could be computed using a detailed heat exchanger model, such as the one presented in Section 2. If the available information is insufficient for this calculation, estimations based on similar heat exchanger models can be used without significantly compromising accuracy, as demonstrated in this section. Besides the temperature and mass flow rate measurements, this simplified model only requires the metal mass of the heat exchanger. If not available, calibration on a dynamic scenario is required. This is not covered in this study.

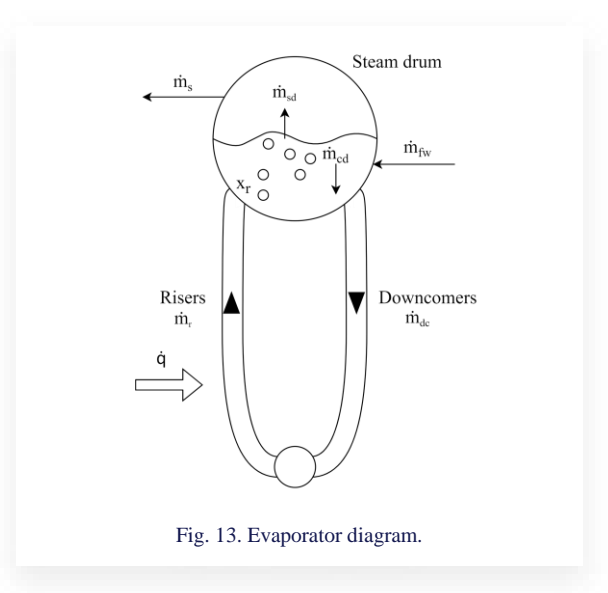


### 3. Evaporator

This section details the model of a natural circulation evaporator-drum based on the work presented in [18]. First, a general description of the system is shown. Then, the main equations that describe the behaviour of the system are listed. Finally, a Modelica model is validated by comparing its results with those presented in the literature using the same parameters.

# 3.1. General description

Figure 13 shows a diagram of the evaporator-drum system and its working principle. Pre-heated feedwater from the economizers enters the drum and mixes with the saturated liquid. The downcomers are vertical tubes connecting the drum to the risers and allowing the recirculation. They are placed outside the HRSG casing, allowing heat transfer to be neglected in this part of the system. The risers consist of finned tubes through which the two-phase water flows and exchange heat with flue gas. In other words, the risers section is the heat exchanger of the system. The drum is the core component. It consists of a thick walled, horizontal, cylindrical tank, in which steam is separated from the mixture by force of density difference between the vapour and liquid phases.



The level of water in the drum is critical for the power plant operation. It is mainly controlled by adjusting the mass flow rate of the feedwater  $\dot{m}_{fiv}$ . Steam bubbles are present below the liquid level of the drum, causing a shrink-and-swell phenomenon when the heat flow varies, which makes the water level control difficult. Modelling this level is therefore mandatory to accurately simulate the behaviour of the system.

Saturated steam flows through the liquid surface in the drum before being extracted and sent to the superheaters. In some cases, saturated steam is sent directly to the steam turbine without superheating. Steam dryers might be implemented to avoid droplets carrying on to the blades.

#### 3.2. Evaporator-drum model

Water and steam occupy the whole volume of the system; therefore, the total volume  $V_{tot}$  of the evaporator-drum can be calculated as

$$V_{tot} = V_{stot} + V_{wtot}, (20)$$

where  $V_{stot}$  and  $V_{wtot}$  represent the total volumes of steam and water, respectively.

Considering the entire system, the global mass and energy balances are given by the following equations:

$$\frac{d}{dt}(\rho_s V_{stot} + \rho_w V_{wtot}) = \dot{m}_{fw} - \dot{m}_s,\tag{21}$$

$$\frac{d}{dt} \left( \rho_s u_s V_{stot} + \rho_w u_w V_{wtot} + m_{wall} C_{p,wall} T_{wall} \right) =$$

$$= \dot{q} + \dot{m}_{fw}h_{fw} - \dot{m}_sh_s, \qquad (22)$$

where  $\dot{q}$  represents the heat flow rate to the risers. Subscripts s, w, and fw denote saturated steam, saturated liquid water and feedwater, respectively. The mass flow rates going in and out of the system are the feedwater  $\dot{m}_{fw}$  and the steam  $\dot{m}_s$ , respectively.

As mentioned earlier, the heat exchange with the flue gas occurs in the risers, which are finned tubes, like the economizers and superheaters. The steam quality increases from the bottom of the risers to their connection with the drum. In [18], a linear mass fraction of steam along the risers is assumed. This assumption fits well with the experimental data, and significantly simplifies the risers' modelling. The average volume fraction can therefore be computed by

$$\overline{x_v} = \frac{\rho_w}{\rho_w - \rho_s} \left[ 1 - \frac{\rho_s}{(\rho_w - \rho_s)x_r} \ln \left( 1 + \frac{\rho_w - \rho_s}{\rho_s} x_r \right) \right]. \tag{23}$$

In this equation,  $\overline{x_v}$  is the average volume fraction of steam in the riser, and  $x_r$  is the steam quality at the riser outlet.

With  $\overline{x_v}$  known, the mass and energy balances on the riser section can be calculated by the following equations:

$$\frac{d}{dt}\left[\rho_s \overline{x_v} V_r + \rho_w (1 - \overline{x_v}) V_r\right] = \dot{m}_{dc} - \dot{m}_r,\tag{24}$$

$$\frac{d}{dt} \left[ \rho_s h_s \overline{x_v} V_r + \rho_w h_w (1 - \overline{x_v}) V_r - P V_r + m_r C_{p,wall} T_{wall} \right] =$$

$$= \dot{q} + \dot{m}_{dc}h_w - (x_r h_c + h_w)\dot{m}_r, \tag{25}$$

$$h_c = h_s - h_w, (26)$$

where  $h_c$  is the condensation specific enthalpy,  $\dot{m}_{dc}$  is the down-comer's mass flow rate,  $V_r$  is the riser tube internal volume and P is the drum pressure.

Recall that downcomers are placed outside the HRSG casing, so the heat transfer in this section can be neglected. However, the dimensions of the downcomers have a major influence on the natural recirculation loop. The flow is driven by the density difference between steam and liquid water in the risers and downcomers. The time constant of the recirculation flow is low, therefore, a steady state relation is used as

$$\frac{1}{2}\zeta\dot{m}_{dc}^2 = \rho_w A_{dc}(\rho_w - \rho_s)g\overline{x_v}V_r, \tag{27}$$

where  $\zeta$  is a dimensionless friction coefficient,  $A_{dc}$  – the down-comers cross-section area, and g – the standard gravitational acceleration.

Considering only the steam under the water level, the mass balance is given by

$$\frac{d}{dt}(\rho_s V_{sd}) = x_r \dot{m}_r - \dot{m}_{sd} - \dot{m}_{cd}, \tag{28}$$

where  $\dot{m}_{sd}$  and  $\dot{m}_{cd}$  represent the steam mass flow rate through the liquid surface and the condensation mass flow rate in the drum, respectively.

The condensation mass flow rate is computed by

$$\dot{m}_{cd} = \frac{h_w - h_{fw}}{h_c} \dot{m}_{fw} + \frac{1}{h_c} \left[ \rho_s V_{sd} \frac{dh_s}{dt} + \rho_w V_{wd} \frac{dh_w}{dt} - (V_{sd} + V_{wd}) \frac{dp}{dt} + m_d C_{p,wall} \frac{dT_{wall}}{dt} \right]. \tag{29}$$

An empirical model that fits well with the experimental data is used to compute the steam flow through the water surface:

$$\dot{m}_{sd} = \frac{\rho_s}{t_d} (V_{sd} - V_{sd}^0) + x_r \dot{m}_{dc} + x_r \beta (\dot{m}_{dc} - \dot{m}_r) \quad (30)$$

with  $V_{sd}^0$  – the volume of steam in the drum when no condensation is occurring,  $t_d$  – the residence time of the steam in the drum and  $\beta$  a constant parameter.

The liquid water in the drum is calculated by

$$V_{wd} = V_{wtot} - V_{dc} - (1 - \overline{x_r})V_r.$$
 (31)

The drum is considered a horizontal cylinder. The volume of water and steam under the drum level can be calculated as a function of the level:

$$V_{wd} + V_{sd} = \left[ \pi r_d^2 - \cos^{-1} \left( \frac{r_d - l}{r_d} \right) r_d^2 - (r_d - l) \sqrt{(2r_d l - l^2)} \right] L_d, \quad (32)$$

where  $r_d$  is the drum radius, l is the water level in the drum, and  $L_d$  is the drum length.

The heat exchange model in the risers is based on the simplified approach presented in Section 2.4. As mentioned earlier, the heat transfer coefficient of the water side is much higher than that of the flue gas side. Therefore, this coefficient is correlated to the flue gas mass flow rate.

#### 3.3. Model validation

The model of the evaporator-drum presented earlier is implemented in Modelica. It was validated by comparing the simulated response of the system to the results presented in [18]. Step changes of the inputs were applied to the model, and the evolution of the outputs was observed. The simulation starts from steady state and at t = 50 s a step change is applied to a single input.

It was necessary to have the same parameters as in [18]. Some of them were explicitly given and used. The remaining parameters and inputs, all of which are listed in Table 3, were calculated based on the steady-state period. For the sake of validation, the following relation is applied:

$$l = \frac{V_{wd} + V_{sd}}{A_d} \tag{33}$$

to link the level to the volume in function of the drum area  $A_d$  at nominal operating level, as in [18]. For real applications, Eq. (32) is used.

A 10 MW step increase to the heat flow to the risers is applied. All other inputs ( $\dot{m}_{fw}$ ,  $\dot{m}_s$  and  $T_{fw}$ ) are kept constant. The step increase of the heat flow, as well the responses of other variables are shown in Fig. 14. Since the steam and the feedwater flows are constant inputs, and the steam generation accelerates with the increased heat flow, the drum pressure builds up linearly. The steam quality at the risers outlet initially increases rapi-

Table 3.	Evaporator-drum	parameters t	for	validation
Table 5.	Lyaporator aram	parameters	LOI	vandation.

Parameter	Symbol	Value	Unit
Drum volume	V <sub>d</sub>	40	m³
Risers volume	Vr	37	m³
Downcomer volume	V <sub>dc</sub>	11	m³
Drum area	Ad	20	m²
Total mass	m <sub>t</sub>	300 000	Kg
Risers mass	m <sub>r</sub>	160 000	kg
Friction coefficient	ζ	25	
Constant parameter	в	0.3	
Residence time	t <sub>d</sub>	12	S
Heat flow	ġ	85.2	MW
Feedwater flow	ṁ <sub>fw</sub>	50.5	kg/s
Steam flow	ṁs	50.5	kg/s
Feedwater temperature	$T_{fw}$	242	°C
Theoretical volume of steam	$V_{sd}^0$	7.6	m³

dly before slowing down with the adaptation of the recirculation flow. The step increase in the heat flow disturbs the balance of the mass flow rates in the risers and downcomers due to the sudden change in density. After about 25 s, the balance is restored. Both mass flow rates decrease linearly with increasing pressure, due to the linear decrease in density difference between saturated liquid and vapour. The drum level undergoes an initial rapid increase, which corresponds to the 'swell' phenomenon. It is caused by accelerated steam generation, which shortly increases the volume of steam under the water surface. The increasing pressure slows down the level increase by reducing the volume of steam and increasing the condensation flow.

These results are consistent with the conclusions of [18]. It should be noted that in this reference, the model was validated on real data from a power plant. The main challenge of this model is to have a good estimation of the residence time  $t_d$  and the constant parameter  $\beta$ . Their calibration is not covered by this study.

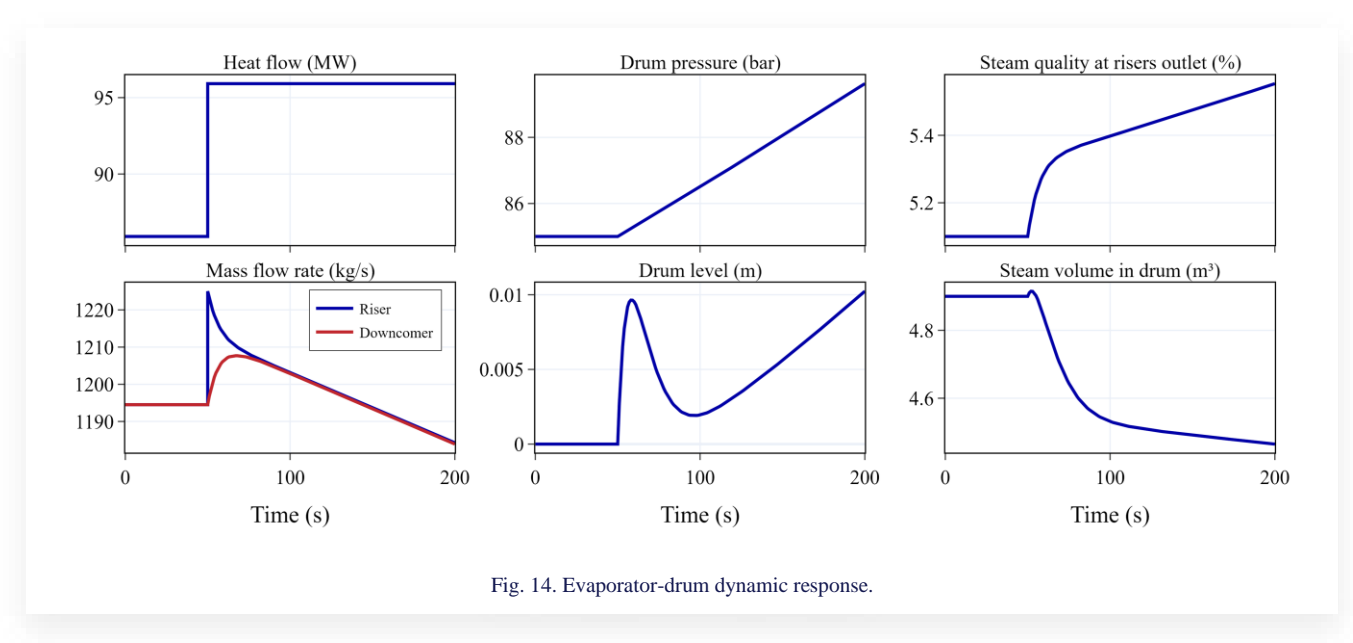
# 4. Full heat recovery steam generator model

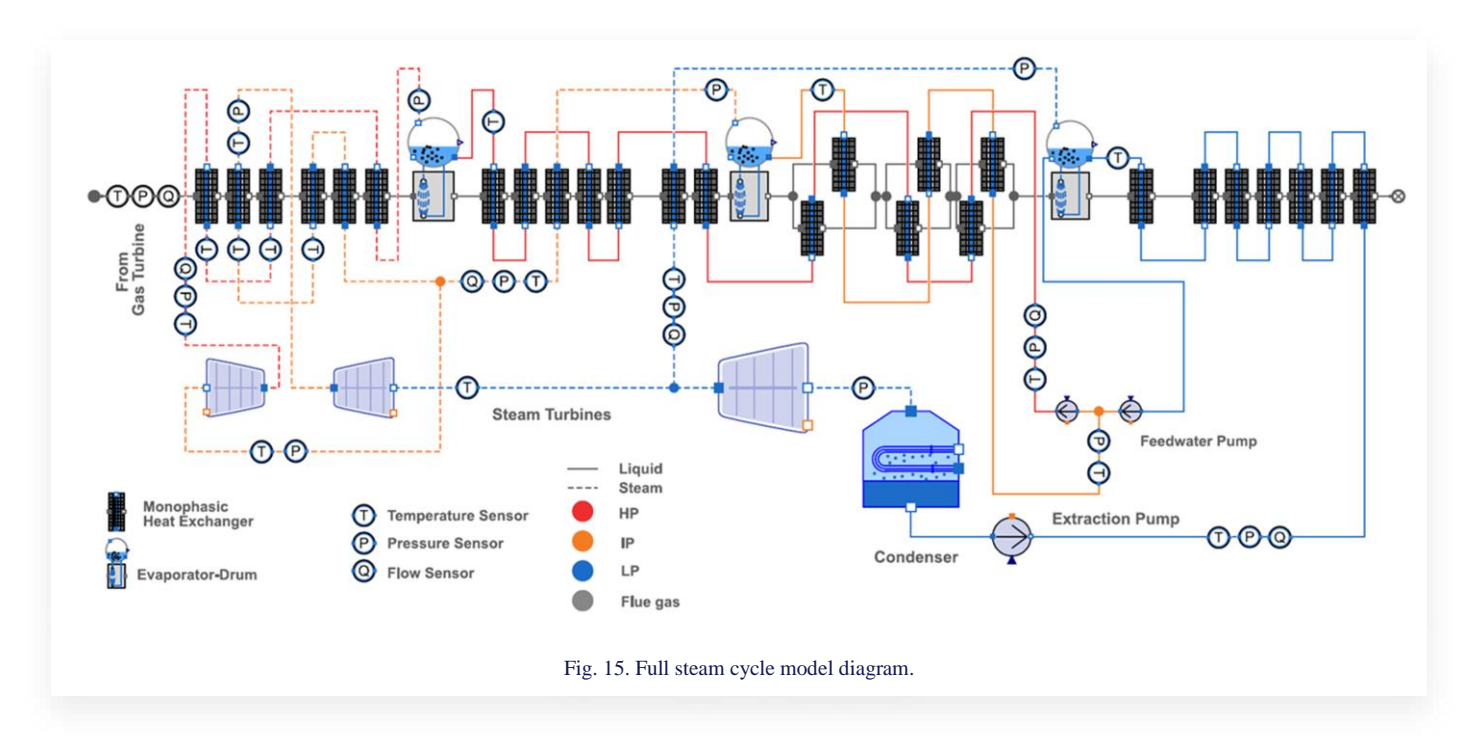
In this section, a full dynamic model of an industrial heat recovery steam generator (HRSG) is developed and simulated. Its diagram is shown in Fig. 15. The monophasic heat exchangers and the drum-evaporator models are based on the methodologies presented earlier. First, a description of the power plant is given. The model is then developed. Finally, the dynamic response is assessed by applying a step increase in the flue gas mass flow rate. The control system is not included in this model, thereby limiting the scope of the analysis to the free response.

#### 4.1. Power plant description

In the context of this study, a collaboration with a CCGT power plant has been established to validate the proposed methodology. It has a 1–1–1 (one gas turbine, one HRSG and one steam turbine line), multi-shaft (two generators: one for the gas turbine and one for the steam turbine) configuration. Due to the significantly fast response of the gas turbine compared to the steam cycle, it has been excluded from the scope of this study. Therefore, the exhaust temperature and mass flow rate will be used as boundary conditions at the inlet of the HRSG, with the exhaust flow rate serving as an indicator of the power plant's load. The HRSG has three natural-circulation evaporator-drum systems, at different pressure levels to maximize heat recovery: high pressure (HP), intermediate pressure (IP) and low pressure (LP).

The extraction pump supplies liquid water from the condenser to the HRSG. Water is first preheated in a series of 7 economizers before entering the LP steam drum. In addition to saturated steam generation, the LP drum serves as a feedwater tank for the IP and HP circuits. Therefore, a feedwater pump with two pressure levels outlets is supplied directly from the LP drum. This configuration complicates the drum levels control due to its strong interdependencies. The LP steam flows in a superheater before being sent to the LP turbine. The IP line consists of 3 economizers, 1 evaporator-drum, 1 superheater, and 3 reheaters. The HP line consists of 8 economizers, 1 evaporator-drum,





and 3 superheaters. The outlet of the HP turbine mixes with the flow from the IP superheater before being heated in the reheaters. The IP turbine discharges directly to the LP turbine. The condenser finally ensures the condensation of the liquid-vapour mixture at the LP turbine outlet. Several control systems, like flue gas condensation, drum levels and steam de-superheating nozzles, are implemented to ensure safe operation. Since the control system is not covered, these systems are excluded.

#### 4.2. Model

The HRSG consists of 26 monophasic heat exchangers and 3 drum-evaporators. The monophasic heat exchangers are modelled based on the simplified approach presented in section 2.4. Therefore, an average flue gas temperature is applied between heat exchangers, which are considered single-pass ones. The tubes are discretized into 6 elements. A global heat transfer coefficient UA, as well as a ratio between the water and flue gas coefficients  $r_{UA}$  is applied for each heat exchanger. Using the sensor measurements, the UA can be determined. However, some heat exchangers are not fully instrumented; therefore, assumptions must be made, such as assigning equal coefficients or using other estimates based on the available design information. The mass of each heat exchanger is obtained from design data, as its calibration falls outside the scope of this study.

Reminding the simplification process of monophasic heat exchanger, the 5th HP economizer is given as an example. It has a 3-row, 4-pass configuration. First, the temperature of the wall is considered uniform. Instead of the 4-pass configuration, a single-pass assumption is adopted, implying that temperatures remain uniform across the width of the heat exchanger. Finally, the heat exchanger is modelled as a discretized tube, with a global heat transfer coefficient UA and a ratio  $r_{UA}$ . Using the outlet water temperature as an input, the overall heat transfer coefficient can be calculated. Its mass is applied from the manufacturer data.

Evaporator-drum systems are modelled based on Section 3. The risers heat exchange module is also based on a simplified approach, as presented in section 2.4. The dimensions and masses for the components are obtained from design datasheets. Since the level is an important parameter of the power plant operation, its modelling is crucial for an accurate representation. Therefore, further simplifications are not possible.

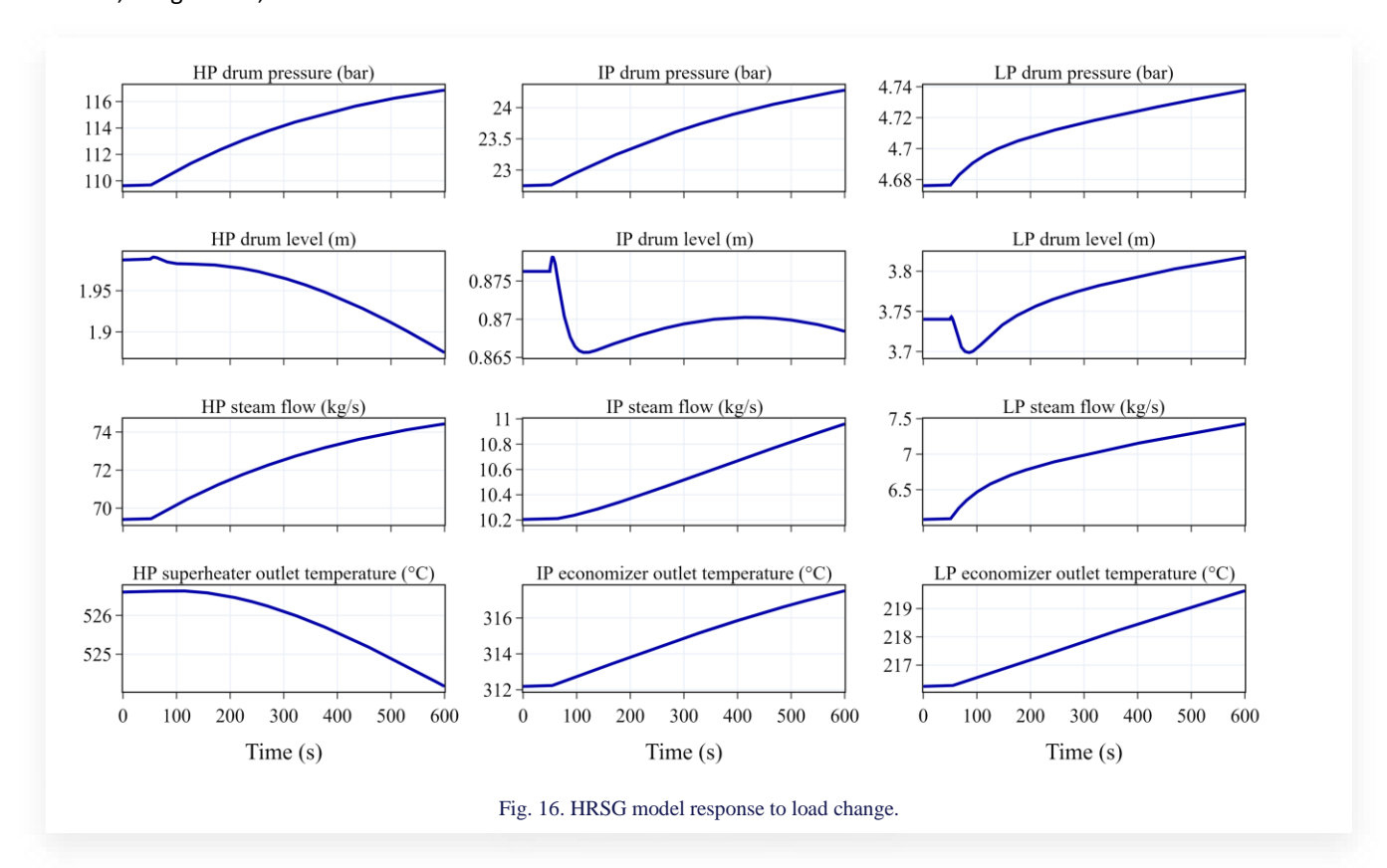
The condenser is also built as a simplified model. The turbine and pumps have low inertia compared to the heat exchangers, therefore their inertia is neglected. Their parameters are calibrated based on operational data.

In terms of causality, the model uses the gas turbine exhaust mass flow rate and temperature, the condenser cooling loop inlet temperature, and the atmospheric pressure as input boundary conditions. Since the control system is not included, the feedwater mass flow rates of the different pressure levels are also imposed as inputs. The model is able to predict all the states of the cycle, including the key measured variables, such as temperatures, pressures, and water levels in the HRSG, as seen in Fig. 15.

# 4.3. Response to step increase in power

The free response of the steam cycle, without including the control system is analysed. A step increase in the mass flow rate of the flue gas from the gas turbine exhaust is applied at t = 50 s, representing a gas turbine load increase. The feedwater mass flow rates are maintained constant, allowing the level to fluctuate freely.

Figure 16 shows the evolution of different variables in function of time. The three drum pressures increase gradually due to the increase in steam generation in the risers section. In the three drums, the swell phenomenon initially appears due to the fast increase of steam volume under the water. The condensation in the drum also increases with increasing pressure, contributing to the water volume in the drums. However, the increasing pressure shrinks the steam volume. The steam mass flow rate in-



creases due to the increase in the pressure difference between the drums and the condenser. If run for a longer time with a constant feedwater flow, all three drum levels will fall to zero. Figure 16 also shows the evolution of three temperatures. The HP superheater outlet temperature slowly decreases with time, due to the increase in the HP steam flow. The HP and IP economizers outlet temperature gradually increase due to increased flue gas mass flow rate and constant feedwater mass flow rates.

The simulation time is extended till the system reaches a new steady state. It should be noted that the drums levels keep decreasing due to the difference between the steam and feedwater flows. The water temperature sensors at the outlet of the heat exchangers and the drum pressure sensors were used to compute the time constants of the heat exchangers. The results are shown in Table 4. The time constants vary between 6 and 73.5 min, which is a much higher order of magnitude compared to the individual heat transfer time constants calculated in the first section. This shows that the delay is propagated in the HRSG, with strong interdependencies between different heat exchangers. When comparing heat exchangers of the same type across different pressure levels, the HP exchangers show the lowest time constants, followed by the IP exchangers, with the LP exchangers having the highest. Although the thickness of the tube walls increases with pressure, the HP components are closer to the source of the perturbation. While the mass of individual components can significantly influence their response, in interconnected systems, the distance from the perturbation source plays a more critical role in determining the time constant.

The results of this section demonstrate the applicability of the modelling methodology to a real industrial HRSG. The model can predict the complex dynamics of the steam drums,

Table 4. Time constants of different components.

Component	τ (min)
HP superheaters	20
HP evaporator	6
HP economizers	16
Reheaters	34.5
IP superheater	10
IP evaporator	9
IP economizers	17.5
LP superheater	73.5
LP evaporator	10
Preheaters	28

especially its level variations. It can provide predictions of sensors during dynamic operation. Coupled with the steam turbines and the condenser, the steam mass flow rate's dependency on evaporator pressure is also simulated. The delay in reaching a new steady state is well represented with the propagation of time constants throughout the HRSG.

#### 5. Conclusions

This paper proposed a dynamic model of a heat recovery steam generator in the context of reducing the dependency on design information and simulation time. The model balances the numerical simplification and accuracy to capture the main dynamic response indicators after a calibration based on measures. First, a mathematical model of monophasic heat exchanger of HRSG has been presented. The discretization methodology and assumptions are investigated to assess their impact on the model's

steady-state and dynamic responses. For instance, a 3-nodes discretization of the tube wall thickness is sufficient to drastically reduce both the steady-state and dynamic errors. The discretization along the tube length is critical to improve the model's precision. Depending on the required precision, the flue gas temperature between heat exchangers can be averaged with minimal impact on errors. Similarly, multi-pass heat exchangers models can be replaced by equivalent one-pass models with negligible impact on the results. Moreover, a simplified model based on the overall heat transfer coefficient has been developed that requires minimal design information. This model can be easily calibrated using the typical instrumentation on the HRSG, however, a preset value for the ratio of the heat transfer coefficients times the area (UA) of water and flue gas sides should be established. The sensitivity analysis on this ratio shows that when the heat exchanger is discretized, the model achieves good precision across a wide range of guessed values. In the second section, a simple model of an evaporator-drum system based on the literature is presented. The model is then validated by comparison of the simulation results with the literature. Finally, a full model of the steam cycle is developed. The heat exchangers in the HRSG were modelled based on the simplified method presented in the first section. The evaporator-drum systems are based on the model from the second section. The free dynamic response, without any control system influence, is analysed by applying a step increase in the flue gas mass flow rate. The behaviour of the main measurable quantities was studied, as well as the time constants of different components. The results demonstrate that this simplified approach effectively simulates the system's dynamic response while maintaining physical accuracy. The time constants of components show that the distance from the perturbation source has a considerable influence on delay to reach a new steady state. Therefore, HP components have lower time constants, followed by IP and then LP components. To go further in this analysis, a calibration based on real measures should be performed. The control system should be implemented, allowing the model to follow the operation of the HRSG in real time, therefore improving its accuracy for different purposes. After that, data validation can be performed. The reliance on real data measurements for calibrating the parameter UA limits the applicability of this modelling methodology to existing systems equipped with sufficient instrumentation. Consequently, it cannot be employed during the design phase of heat exchangers. Although this approach provides a simplified modelling approach with minimal reliance on design data and enables faster simulations, it should be coupled by a calibration strategy to account for parameter variations under different boundary conditions. This is achieved by the conventional heat exchanger modelling methodologies through empirical correlations that relate the heat transfer coefficient to various operating conditions, such as changes of mass flow rates.

#### References

IEA (2024). Electricity 2024. https://www.iea.org/reports/electricity-2024 [accessed 30 Nov. 2024].

- [2] Holttinen, H. (2012). Wind integration: experience, issues, and challenges. WIREs Energy and Environment, 1(3), 243–255. doi: 10.1002/wene.18
- [3] IRENA (2019). Innovation landscape brief: Flexibility in conventional power plants. International Renewable Energy Agency, Abu Dhabi. https://www.irena.org/-/media/Files/IRENA/Agency/Publication/2019/Sep/IRENA\_Flexibility\_in\_CPPs\_2019.pdf?la=en&hash=AF60106EA083E492638D8FA9ADF7FD099259F5A1 [accessed 25 Oct. 2024].
- [4] Casella, F., & Pretolani, F. (2006). Fast start-up of a combined-cycle power plant: A simulation study with Modelica. 5th International Modelica Conference, Sep. 6-8, Vienna, Austria. https://modelica.org/events/modelica2006/Proceedings/sessions/Session 1a1.pdf [accessed 15 Sept. 2024].
- [5] Alobaid, F., Postler, R., Ströhle, J., Epple, B., & Kim. H.-G. Modeling and investigation start-up procedures of a combined cycle power plant. *Applied Energy*, 85(12), 1173–1189. doi: 10.1016/j.apenergy.2008.03.003
- [6] Benato, A., Stoppato, A., & Bracco, S. (2014). Combined cycle power plants: A comparison between two different dynamic models to evaluate transient behaviour and residual life. *Energy Con*version and Management, 87, 1269–1280. doi: /10.1016/j.enconman.2014.06.017
- [7] Farahani, Y., Jafarian, A., & Mahdavi Keshavar, O. (2022). Dynamic simulation of a hybrid once-through and natural circulation heat recovery steam generator (HRSG). *Energy*, 242, 122996. doi: 10.1016/j.energy.2021.122996
- [8] Jain, P., Poon, J., Singh, J.P., Spanos, C., Sanders, S.R., & Panda, S.K. (2020). A digital twin approach for fault diagnosis in distributed photovoltaic systems. *IEEE Transactions on Power Electronics*, 35(1), 940–956. doi: 10.1109/TPEL.2019.2911594
- [9] Allard De Grandmaison, I., Muszynski, L., & Schwartz, A. (2019). AI diagnosis for maintenance teams: building of a digital twin. *VGB PowerTech*, 99(8), 67–72.
- [10] Mertens, N., Alobaid, F., Starkloff, R., Epple, B., & Kim, H.-G. (2015). Comparative investigation of drum-type and once-through heat recovery steam generator during start-up. *Applied Energy*, 144, 250–260. doi: 10.1016/j.apenergy.2015.01.065
- [11] Dittus, F.W., Boelter, L.M.K. (1985). Heat transfer in automobile radiators of the tubular type. *International Communications in Heat and Mass Transfer*, 12(1), 3–22. doi: 10.1016/0735-1933 (85)90003-X
- [12] Walter, H., & Hofmann, R. (2011). How can the heat transfer correlations for finned-tubes influence the numerical simulation of the dynamic behavior of a heat recovery steam generator? *Applied Thermal Engineering*, 31(4), 405–417. doi: 10.1016/j.applthermal eng.2010.08.015
- [13] Can Gülen, S., & Kim, K. (2014). Gas turbine combined cycle dynamic simulation: A physics based simple approach. *Journal of Engineering for Gas Turbines and Power*, 136(1), 011601. doi: 10.1115/1.4025318
- [14] Dechamps, P.J. (1995). Modelling the transient behaviour of heat recovery steam generators. Proceedings of the Institution of Mechanical Engineers, Part A: Journal of Power and Energy, 209(4), 265–273. doi: 10.1243/PIME\_PROC\_1995\_209\_005\_01
- [15] Modelica Association (2000). ModelicaTM A Unified Object-Oriented Language for Physical Systems Modeling Version 1.4 Tutorial. https://modelica.org/documents/ModelicaTutorial14.pdf [accessed 11 Aug. 2023].
- [16] Dymola Dassault Systèmes. https://www.3ds.com/products-services/catia/products/dymola/ [accessed 18 July 2023].
- [17] Metroscope (2023). Metroscope Modeling Library. https://github. com/Metroscope-dev/metroscope-modeling-library [accessed 18 July 2023].
- [18] Åström, K.J., & Bell, R.D. (2000). Drum-boiler dynamics. *Automatica*, 36(3), 363–378. doi: 10.1016/S0005-1098(99)00171-5